Loadability Maximisation in Bilateral Network for Real-Time Forecasting System Using Cuckoo Search Algorithm

Venkatasivanagaraju S.*, M. Venkateswara RAO

Department of Electrical and Electronics Engineering, Jawaharlal Nehru Technological University Anantapur, Ananthapuramu, India; e-mail: mvrao.eee@jntua.ac.in

* Corresponding Author e-mail: svsivanagaraju1@gmail.com

This manuscript proposes an optimal power flow (OPF) solution in a coordinated bilateral power network. The primary goal of this project is to maximise the benefits of the power market using Newton–Raphson (NR) and cuckoo search algorithm CSA methodologies. The global solution is found using a CSA-based optimisation approach. The study is conducted on real-time bus system. To avoid this, creative techniques have lately been used to handle the OPF problem, such as loadability maximisation for real-time prediction systems employing the CSA. In this work, cuckoo search (CS) is used to optimise the obtained parameters that help to minimise parameters in the predecessor and consequent units of each sub-model. The proposed approach is used to estimate the power load in the local area. The constructed models show excellent predicting performance based on derived performance. The results confirm the method's validity. The outcomes are compared with those obtained by using the NR method. CSA outperformed the other methods in this investigation and gave more accurate predictions. The OPF problem is solved via CSA in this study. Implementing a real-time data case bus system is recommended to test the performance of the established method in the MATLAB programme.

Keywords: optimal power flow, NR method, short-term and long-term load forecasting, cuckoo search algorithm, optimisation and loss minimisation.

1. Introduction

Power system must function at its full capacity under contingencies and emergency situations, and this includes maximising the capacity of the current transmission network to transfer electricity [1, 2]. Chávarro-Barrera *et al.* [3] presented an approach based on technical considerations that was used to de-

termine the increase in loading margin (LM) by deploying different types of flexible AC transmission systems (FACTS) devices in different places. Because it takes several man-hours to locate the appropriate device and its ideal control situations in an optimum position, such a technique is not reliable. A method for calculating LM and static VAR compensator (SVC) settings under contingency scenarios, was proposed by Yang and Suash Deb [4]. To recognise the positions and regulate locations of several FACTS device for LM improvement, a technique based on GA was presented by Gao *et al.* [5]. Certain power system situations, such as unanticipated load increases, the loss of major transmission lines, transformers, or generators, and improper control device operation, affect voltage stability, resulting in reactive power generation limits violations [6]. In voltage collapse analysis, some continuation techniques [7–10] are used to determine the loading margins; such approaches have excellent numerical precision, are dependable, and follow the path from any operating point to the voltage collapse point. However, these solutions take longer and require more knowledge for bigger systems. One of the common methods for determining a system's load capability is to employ typical load flow, and gradually increase loads till convergence is no longer obtained [11, 12]. Because such an approach necessitates physical involvement, it frequently suffers from convergence while working under restrictions. The authors [13–15] showed how to use GA and PSO techniques to find the best site for SVC to improve system load capacity, its power injection model, divergence equations, and inclusion process in the traditional NR load flow. A suitable placement strategy based on bus voltage magnitude fluctuations and transmission line loadings was proposed by Aminifar *et al.* [16] to increase system security by reducing system severity. The distribution of the problem regulator variables is static and the two-stage loading of the variables is taken into account in a novel optimisation method that is presented. The loadability index (LI), a well-known problem, is employed in this study to increase both active and reactive load, and the suggested technique is used to maximise both while meeting equality, inequality, and device operational limitations. The typical IEEE-30 bus system is divided into three zones, and each zone's individual zonal LI fluctuations with and without a generalised unified power flow controller (GUPFC) are examined for regular, potential, and active load differences in order to test the zonal loadability theory and provide supporting evidence.

Researchers have recently shown an interest in incorporating requests into objective functions in order to maximise market profitability. Demand restrictions are also included in the objective function of issues. Customers did not have an effective involvement in power markets in the early days of deregulation, and as a result, they were unable to adjust to the pricing effectively. However, in order to have a fully competitive market, customers must be sufficiently motivated to engage in power market operations [17].

The present research focuses on traffic control in a centralised market with bilateral agreements among generators and customers. The formulation of the problem is founded on benefit maximisation, with customer functions adding to the problem's purpose. For congestion control, the line limitations are also considered in this calculation. The interior point (IP) approach is used to find the answer. Because of its quick computing speed and resilience, this approach has been widely used to address large-scale OPF issues. The calculation of objective function gradient, Jacobian, and Hessian matrices are constraint functions in IP-OPF. The performance of the suggested technique was shown using a modified IEEE-30 bus system. Even when losses in problem formulation are taken into account, the test results show that the suggested technique generates good outcomes [18].

2. NR METHOD USING POLAR COORDINATES

The NR approach may be used to solve the power flow problem when the bus voltages are presented in polar form. In actuality, only the polar form is used in practice since it produces fewer equations than the total amount of equations in rectangular form.

The actual and reactive power flow on distribution lines, reactive power generator buses, and magnitude and phase angle of load bus voltages are among the findings of this study. The terms are confined to first-order approximation in the NR technique of load flow analysis in an equation employing Taylor's series expansion.

The non-linear equation of the leading power system is:

$$S_k = V_k I_k^* = P_k + jQ_k, \tag{1}$$

since S_k is the rectangular power in bus k, and V_k is bus voltage at k is specified as:

$$V_k = |V_k|e^{-i\sigma j}, \tag{2}$$

$$V_k^* = |V_k|\,e^{-j\sigma i}, \tag{3}$$

σi is the bus angle at node i, σj is the bus angle at node j, V_k^* is the rectangular bus voltage at node k, V_k is the bus voltage at k, and I_k is the current injected into bus k and is given by:

$$I_k = \sum_{k=1}^{n} V_k Y_{kl}, \qquad k = 1, 2, ..., n, \tag{4}$$

$$Y_{lk} = |Y_{lk}|e^{-l\theta_{kl}}, \tag{5}$$

Y_{lk} is the "admittance" at buses l and k, θ_{kl} is "admittance" angle at junctional k.

P_k, Q_k is the true and wattless power at bus k,

$$S_k^* = V_k * I_k = P_k - jQ_k = \sum_{k=1}^{n} |V_k| \, |V_l| \, |Y_{lk}| e^{-j(\theta_{lk} + \sigma_k - \sigma_l)}, \tag{6}$$

the distinct conjugate solution of S_k^* is the true and wattless power

$$P_k = \sum_{i=1}^{n} |V_k| \, |V_l| \, |Y_{lk}| \cos(\theta_{lk} + \sigma_k - \sigma_l). \tag{7}$$

Calculate and add P_k for $k = i$ and for $k \neq i$:

$$P_k = V_k^2 Y_{kk} \cos \theta_{kk} + \sum_{k=1, k \neq 1}^{n} |V_k| \, |V_l| \, |Y_{kl}| \cos(\theta_{kl} + \sigma_k - \sigma_l). \tag{8}$$

Similarly,

$$Q_k = V_k^2 Y_{kk} \sin \theta_{kk} + \sum_{k=1, k \neq 1}^{n} |V_k| \, |V_l| \, |Y_{kl}| \sin(\theta_{kl} + \sigma_k - \sigma_l). \tag{9}$$

Equations (8) and (9) constitute the polar form of the power flow equation that provide the calculated values for the net real power P_k and reactive power Q_k entering the network at bus k.

Denoting the calculated values of P_k by P_{kcal} and Q_k by Q_{kcal} leads to the definition of mismatches ΔP_k and ΔQ_k:

$$\Delta P_k = P_{ksch} - P_{kcal}, \tag{10}$$

$$\Delta Q_k = Q_{ksch} - Q_{kcal}, \tag{11}$$

$$P_{ksch} = P_{gk} - P_{dk}, \tag{12}$$

$$Q_{ksch} = Q_{gk} - Q_{dk}, \tag{13}$$

where P_{ksch} and Q_{ksch} are the net true, reactive and planned power injections into bus k, P_{gk} and Q_{gk} denote the planned true and reactive produced power at bus k, and P_{dk} and Q_{dk} represents the planned true and wattless power request at load bus k. Mismatches occur when P_{kcal} and Q_{kcal} do not match the planned values.

The linear equations interrelating the changes in power with change in real and reactive components of the bus voltages can be written in polar form as:

$$\begin{bmatrix} \Delta P_k \\ \Delta Q_k \end{bmatrix} = \begin{bmatrix} J_{11} & J_{12} \\ J_{21} & J_{22} \end{bmatrix} \begin{bmatrix} \Delta \sigma_k \\ \Delta V_k \end{bmatrix}, \tag{14}$$

where matrix J_{11}, J_{12}, ... are a separated matrix by the resolution in the method:

$$
\begin{bmatrix}
\dfrac{\partial P}{\partial \sigma} & \dfrac{\partial P}{\partial |V|} \\[3mm]
\dfrac{\partial Q}{\partial \sigma} & \dfrac{\partial Q}{\partial |V|}
\end{bmatrix}.
\tag{15}
$$

The σ_k and $|V_k|$, are obtained with the help of can be obtained by expressing the linear (14) as:

$$
J_{11} = \frac{\partial P}{\partial \sigma}
\begin{bmatrix}
\dfrac{\partial P_k}{\partial \sigma_k} & \cdots & \dfrac{\partial P_k}{\partial \sigma_n} \\[3mm]
\vdots & \ddots & \vdots \\[3mm]
\dfrac{\partial P_n}{\partial \sigma_k} & \cdots & \dfrac{\partial P_n}{\partial \sigma_n}
\end{bmatrix},
\tag{16}
$$

$$
J_{12} = \frac{\partial P}{\partial |V|}
\begin{bmatrix}
\dfrac{\partial P_k}{\partial |V_k|} & \cdots & \dfrac{\partial P_k}{\partial |V_n|} \\[3mm]
\vdots & \ddots & \vdots \\[3mm]
\dfrac{\partial P_n}{\partial |V_k|} & \cdots & \dfrac{\partial P_n}{\partial |V_n|}
\end{bmatrix},
\tag{17}
$$

$$
J_{21} = \frac{\partial Q}{\partial \sigma}
\begin{bmatrix}
\dfrac{\partial Q_k}{\partial \sigma_k} & \cdots & \dfrac{\partial Q_k}{\partial \sigma_n} \\[3mm]
\vdots & \ddots & \vdots \\[3mm]
\dfrac{\partial Q_n}{\partial \sigma_k} & \cdots & \dfrac{\partial Q_n}{\partial \sigma_n}
\end{bmatrix},
\tag{18}
$$

$$
J_{22} = \frac{\partial Q}{\partial |V|}
\begin{bmatrix}
\dfrac{\partial Q_k}{\partial |V_k|} & \cdots & \dfrac{\partial Q_k}{\partial |V_n|} \\[3mm]
\vdots & \ddots & \vdots \\[3mm]
\dfrac{\partial Q_n}{\partial |V_k|} & \cdots & \dfrac{\partial Q_n}{\partial |V_n|}
\end{bmatrix}.
\tag{19}
$$

The solution for $\Delta\sigma_k$, ΔV_k given to Eq. (19) is to be useful to correct $|V_k|$ and σ_k:

$$
\begin{aligned}
|V_k|^{(a+1)} &= |V_k|^{(a)} + \Delta |V_k|^{(a)}, \\
\sigma_k^{(a+1)} &= \sigma_k^{(a)} + \Delta\sigma_k^{(a)}.
\end{aligned}
\tag{20}
$$

The NR technique is used to explain the polar variant of linearisation until all bus mismatches are within the specified tolerances.
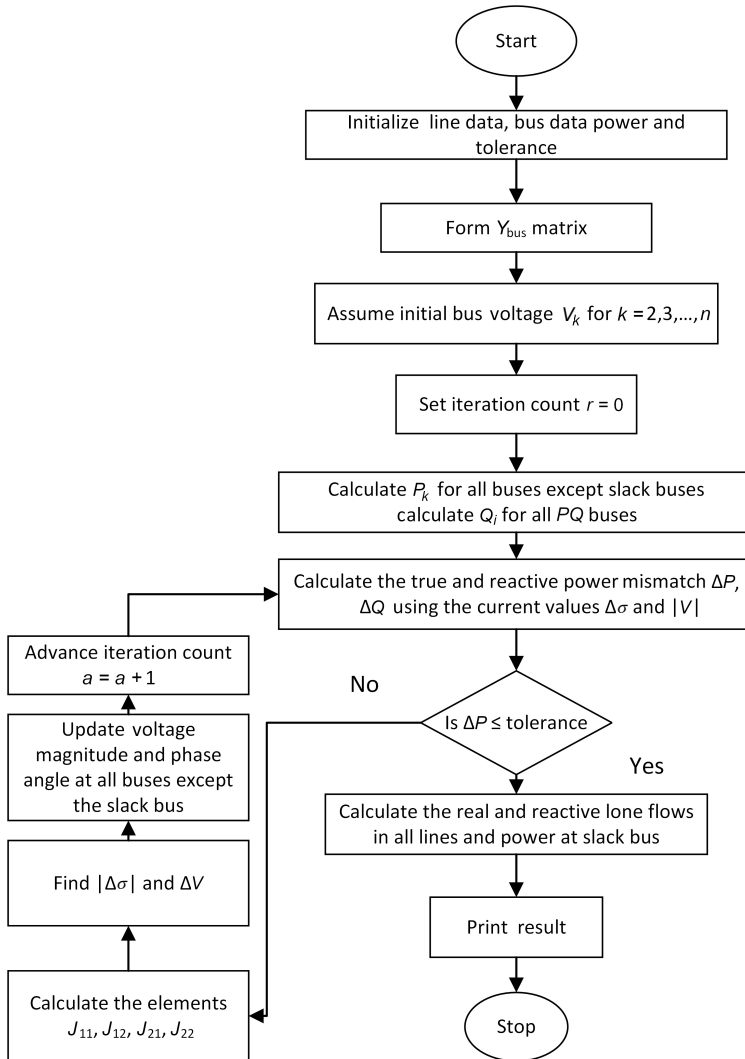
Fɪɢ. 1. Flowchart of NR approach.

2.1. The NR algorithm

STEP 1: Create the Y-bus matrix.

STEP 2: Assume that the magnitude of the bus voltage, $|V_k|$, and its phase angle, k are both equal to slack values. In most cases, $|V_1| = 1.00$ pu and $1 = 0$ radians.

STEP 3: Set the iteration count to zero $(a = 0)$.

STEP 4: Using Eqs. (20) and (21), compute the true and reactive power for each load bus.

STEP 5: Using Eqs. (22) to (25), calculate planned errors for each load bus. If a bus is powered by a generator (PV), calculate only the change in real power because the value of reactive power is within its limits. If it goes beyond the bounds, regard the limit that was breached as reactive power and treat it like a *PQ* bus.

STEP 6: Using the estimated $|V_k|$ and k from step 2, calculate the Jacobian matrix elements.

STEP 7: Determine the values of $|V_k|$ and k.

STEP 8: Modify $|V_k|$ and k at all loads using the values of $|V_k|$ and k acquired in step 7. With the updated values of $|V_k|$ and k begin the next iteration cycle at step 2.

STEP 9: Repeat until all planned errors for all load buses are under a given error tolerance, i.e., $P_k(a)$, $Q_j(a)$, where r is the load bus tolerance level.

STEP 10: Calculate the slack bus line flows and power.

2.2. OPF problem formulation

The OPF problem considers non-linearities and complexity when optimising power system objectives. Finally, while fulfilling equality, inequality, and device operating requirements, a collection of control variables is derived as a solution for the problem. The system's active and reactive power LI is optimised for the loadability problem. The LI is gradually increased from its starting point until the transmission line and bus voltages are violated. The following is a mathematical formulation of the problem as a constrained nonlinear objective optimisation problem:

Consider a radial distribution network with a number of buses k and an established distribution arrivals E linking them. It defines buses in k of $k = 0, 1, ..., n$, where n is a line in E of the pair (k, l) of connection buses, and k symbolizes the bus nearest to the power source. Each of the other buses: $k \in N \backslash \{0\}$ represents a collector that can contribute to the solution to the query. Slack bus is a bus that needs constant voltage but allows for variable energy injection to balance the charges.

We will refer to the aggregator's user kin that, in actuality, signifies a collection of clients who are linked to the bus and who join the scheme to answer query as a single object. Let $Z_{k,l} = r_{k,l} + ix_{k,l}$ be a line impedance (k, l), $S_{k,l} = P_{k,l} + iQ_{k,l}$ a rectangular power, and $I_{k,l}$ the current flowing from bus k to bus l for the individual link $(k, l) \in E$.

Leave $S_k = p_k + iq_k$ as the composite load and V_k as the composite voltage for each bus. We assume that the composite voltage V_0 in the power supply is

determined and preset, as is customary. For each $(k,l) \in E$, the bifurcation flow model, initially presented in [12], represents the power currents in a fixed point in a radial supply system:

$$\frac{(P_{k,l}^2 + Q_{k,l}^2)}{v_k} = l_{k,l}, \tag{21}$$

$$P_{k,l} = \sum_{(k,l) \in E} P_{k,l} + r_{k,l} l_{k,l} + p_l, \tag{22}$$

$$Q_{k,l} = \sum_{(k,l) \in E} Q_{k,l} + x_{k,l} l_{k,l} + q_l, \tag{23}$$

$$v_k + v_l = 2\left(r_{k,l} P_{k,l} + x_{k,l} Q_k\right) - \left(r_{k,l}^2 + x_{k,l}^2\right) l_{k,l}, \tag{24}$$

where $l_{k,l} := |I_{k,l}|^2$, $v_k = |v_k|^2$ and $k \in N \backslash \{0\}$. When a user's active power utilization is p_k, it reaches a particular utility $f_k(p_k)$. Typically, the utility function $f_k(p_k)$ is left undefined and assumed to be continuous, increasing, and coiled. In addition, for each $k \in N \backslash \{0\}$ there is a further operational restriction:

$$\underline{v_k} \leq v_k \leq \overline{v_k} k = 1, ..., n, \tag{25}$$

$$\underline{q_k} \leq q_k \leq \overline{q_k} k = 1, ..., n, \tag{26}$$

$$\underline{p_k} \leq p_k \leq \overline{p_k} k = 1, ..., n. \tag{27}$$

The radial distribution system receives power from the primary grid all the way via the line (i.e., zero bus). Total (true) power supply P_0 stands specified through $P_0 = \sum_{k:(0,k) \in E} P_{0,l}$. Consider a scenario where the power supply P_0 is constrained by an upper bound $\overline{P_0}$, i.e.,

$$P_0 = \sum_{k:(0,k) \in E} P_{0,k} \leq \overline{P_0}. \tag{28}$$

In this case, the layout of a networked appliance should direct each user k to select a suitable load P_k, ensuring that the supply limit (30), the power flow and the working limitations planned in (22)–(29) are met and the problem is expressed using the OPF below:

$$\text{OPF} : \max \sum_{k=1}^n f_k(p_k) - C_0(P_0) - \rho \sum_{(k,l) \epsilon E} r_{k,l} l_{k,l}. \tag{29}$$

3. CUCKOO SEARCH METHODOLOGY

Researchers are interested in the Cuckoo search algorithm (CSA) because it provides the effectiveness in practical applications and capacity to address a range of optimal problems. The traditional CS is described by the following two rules [4]: The nests with the best eggs are handed down to the next phase; the bird discovers cuckoo's egg with a probability for paternity (0, 1). In this case, the host bird must decide whether to remove the egg or depart the nest. The CS method is depicted as a flowchart in Fig. 2 based on two already defined criteria. The ability of the changing variable to combine locally and globally random walks separates CSA from additional similar algorithms, making it faster to reach global optima. The switching parameter $P_a \in [0, 1]$ is conceptually tied to Eq. (31) and determines the balance between local and global random walks (31):

$$v_i^{t+1} = v_i^t + \alpha s H(P_a - \epsilon) X(v_k^t - v_l^t), \tag{30}$$

$$v_i^{t+1} = v_i^t + \alpha L(m, \lambda), \tag{31}$$

where v_i^{t+1} is an updated position, and v_k^t, v_l^t are the present positions chosen by arbitrary variation, is stepwise creation of multiple paths, m is step size, H is the heavy-side function, P_a is the switching parameter between local and global random walks, and is a random integer from uniform distribution. A random walk's step size is defined by the Lévy distribution $L(m, \lambda)$ and α is the step size which should be related to the scales of the problem of interests. Lévy flights essentially provide a random walk for huge steps, with its casual stages produced from a Lévy delivery. The most successful technique for making step weights is to use Mantegna's equations with the gamma distribution described by:

$$\lambda = \left\{ \left| \left[\Gamma(1+\beta) \sin\left(\Pi\beta/2\right) \right] \middle/ \left[\gamma(1+\beta)/2\beta \cdot 2^{\alpha-1/2} \right] \right| \right\}^{1/\beta}, \tag{32}$$

where $\gamma[\,]$ is the distribution function and $\beta = 3/2$.

3.1. Solution approach using CSA

This section discusses the multi-objective problem's control parameters and the general method for solving the suggested fitness function. This article examines changes in generation and loading situations with proper management in order to minimise voltage deviation vs. reference voltage, actual power loss, and outage point signalling. Traditional energy generation, generator bus voltage magnitudes, tap-changer settings, and shunt MVAR (megavolt-amperes) injection are among the control factors. If it is in good condition, that is an advantage. In each cycle, the system bus data and line data are refreshed with new data,

including generator bus voltage magnitudes, tap-changer ratios, shunt MVAR injections, system regulating variables, and power injections at their incident buses. To evaluate the overall unbiased function specified in Eq. (33), the NR power flow explanation is used to compute the total true power loss, regular VCPI, and normal voltage deviation index (10).
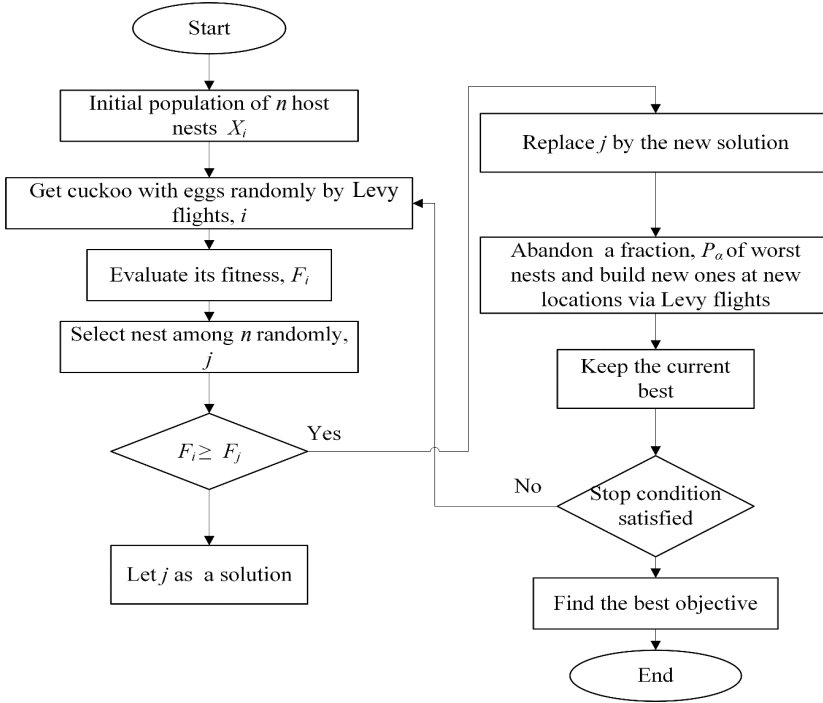
FIG. 2. Flowchart for CSA approach for solving OPF problem.

4. ANALYSIS FOR REAL-TIME DATA

4.1. Realistic load modelling

In traditional load flow analyses, true and imaginary power needs are considered to have constant values, independent of voltage magnitude on the same bus. Different types and classifications of loads may be present in the actual power system operation. The active and reactive powers of these sorts of loads depend on the voltage and frequency of the system and are evaluated in various design situations. Constant power, industrial, residential, and commercial loads are examples of realistic loads. The load models can be stated quantitatively as:

$$P_L = P_{L_0} \times \left(\frac{V}{V_0}\right)^{\alpha},\tag{33}$$

$$Q_L = Q_{L_0} \times \left(\frac{V}{V_0}\right)^{\beta}, \tag{34}$$

where α and β are the load exponents, and P_{L_0} and Q_{L_0} are the active and reactive power values at nominal voltages, respectively. The load bus voltage and nominal voltage are represented by V and V_0, respectively. Table 1 shows the standards of the real and reactive components used in this study for domestic, industrial, and commercial loads.

TABLE 1. Real and reactive components.

Load component	α	β
Domestic	0.91	4.03
Industrial	0.17	5.99
Commercial	1.50	3.39

4.2. Load growth

For arrangement and growth or a well-organized process of distribution networks, a system engineer should know the future estimation of the systems solutions. Load increase is modelled as follows in the suggested load flow algorithm:

$$\text{Load} = \text{Load} \times (1 + (h/100))^{n}, \tag{35}$$

where h is the yearly load development rate of 7.5% and n is the number of years.

4.3. Projected approach

In this work, the influence of different load representation is examined by implementing the Andhra Pradesh Southern Power Distribution Corporation Limited (APSPDCL) distribution systems in Chittoor District, India. Load flow analysis is performed for each load model. The data of ten years is used to attain the required outputs. The impact of load models is examined by calculating active power loss P_L and active power intake P_{intake} in the tested distribution structure. The variance between the characteristics is derived to evaluate the performance of load models for the tested distribution structure.

4.4. Power loss reduction

Through a load flow analysis the electric active power loss of the system is calculated and expressed as:

$$P_L = \sum_{i=1}^{n} i^2 R_i, \tag{36}$$

where n is the number of distribution system branches, i is the current flowing through each branch, and R_i is the resistance of each branch.

4.5. Active power demand

The active power intake P_{intake} can be calculated by adding power losses and true power demands by all buses in the distribution structure. This can be expressed by using the following equation:

$$P_{\text{intake}} = P_D + P_L. \tag{37}$$

5. Results and discussions

5.1. Time-varying base load model

Table 2 show transmission power loss (TPL) minimisation and loadability maximization for STLF: base case. For the whole period, there is a significant decline in the MVAR system.

Table 2. TPL minimisation and loadability maximization for STLF: base case.

Month	Base case [in MW]					
	TPL minimisation			Loadability maximisation		
	Load	Loss		Loadability	Load	Loss using OPF
		Load flow	OPF			
January	1383.9	68.1822	42.292	0.9157	1509.532	46.16468
February	1385.0	68.6508	42.729	0.7922	1494.720	46.11399
March	1388.3	69.4707	42.408	0.9595	1521.507	46.47705
April	1389.9	69.9280	42.682	0.6557	1481.036	45.48066
May	1395.7	71.6703	43.620	0.5570	1473.440	46.04963
June	1397.1	72.0901	41.715	0.8491	1515.728	45.25702
July	1398.7	72.5862	42.950	0.6340	1487.378	45.67303
August	1399.9	72.9680	43.472	0.6787	1494.911	46.42244
September	1401.5	73.4871	42.745	0.3577	1451.632	44.27399
October	1404.5	74.5150	41.916	0.3431	1452.688	43.35414
November	1406.7	75.2814	42.930	0.3922	1461.871	44.61371
December	1413.2	77.7635	41.744	0.6555	1505.835	44.48032

5.2. Time-varying composite load mode

According to Table 3 the decrease in P_{intake} and energy losses for the time flexible composite load model is substantial. However, as it is shown the decline

TABLE 3. TPL minimisation and loadability maximization for STLF: composite load.

	Load	Load flow loss	OPF Loss	Loadability	Load	Loss
Month	Composite load [in MW]					
January	1386.4	69.105	53.1624	0.1712	1410.135	54.07254
February	1389.9	69.929	52.4332	0.7060	1488.027	56.13498
March	1390.6	70.141	52.0968	0.0318	1395.022	52.26247
April	1391.4	70.364	52.0346	0.2769	1429.928	53.47544
May	1391.8	70.493	52.9497	0.0462	1398.230	53.19433
June	1394.6	71.333	52.6582	0.0971	1408.142	53.16951
July	1397.8	72.296	52.0791	0.8235	1512.909	56.36781
August	1400.3	73.111	52.5405	0.6948	1497.593	56.19101
September	1405.7	74.912	52.9235	0.3171	1450.275	54.60170
October	1410.1	76.525	51.8106	0.9502	1544.088	56.73364
November	1415.5	78.755	52.6013	0.0344	1420.369	52.78225
December	1422.1	82.287	53.7979	0.4387	1484.488	56.15801

pattern of load models is inconsistent throughout the months. Table 3 demonstrates also the losses for composite load models, for the short-term loading forecast (STLF) scenario between January 2020 to December 2020.

Tables 4 and 5 illustrate the observations for long-term loading forecast (LTLF), covering load increases and reductions between 2020 to 2030. They show transmission power loss (TPL), minimization and loadability maximization for LTLF.

TABLE 4. TPL minimisation and loadability maximization for LTLF: base case.

Year	Base case [in MW]					
	TPL minimisation			Loadability maximisation		
	Load	Loss		Loadability	Load	Lossusing OPF
		Load flow	OPF			
2020	1395.1	71.4698	52.4872	0.3816	1448.337	54.49011
2021	1401.3	73.4437	53.3874	0.7655	1508.570	57.47421
2022	1422.6	82.6578	53.6397	0.7952	1535.725	57.90513
2023	1395.4	71.5511	52.6150	0.1869	1421.480	53.59837
2024	1405.1	74.7140	52.5576	0.4898	1473.922	55.13187
2025	1416.6	79.2250	53.4708	0.4456	1479.724	55.85346
2026	1423.9	83.9394	50.5654	0.6463	1515.927	53.83344
2027	1421.0	81.5588	53.1220	0.7094	1521.806	56.89047
2028	1418.5	80.1559	52.9828	0.7547	1525.554	56.98141
2029	1424.3	84.6615	51.6304	0.2760	1463.611	53.05540
2030	1408.2	75.8217	52.9394	0.6797	1503.915	56.53769

TABLE 5. TPL minimisation and loadability maximization for LTLF: load growth.

Year	Load growth [in MW]								
	TPL minimisation					Loadability maximisation			
	Load	Loss	Status	Loss	Status	Loadability	Load	Loss	Status
		Load flow		OPF				OPF	
2020	1387.0	69.117	C*	52.2672	C	0.1626	1409.553	53.11706	C
2021	1392.6	70.715	C	51.9295	C	0.1190	1409.172	52.54746	C
2022	1398.1	72.415	C	53.0783	C	0.4984	1467.781	55.72372	C
2023	1403.7	74.245	C	52.2063	C	0.9597	1538.413	57.21654	C
2024	1409.4	76.250	C	51.5334	C	0.3404	1457.376	53.28760	C
2025	1415.0	78.520	C	53.8582	C	0.5853	1497.820	57.01052	C
2026	1420.6	81.335	C	55.4283	C	0.2238	1452.393	56.66879	C
2027	1426.3	–	D**	72.7635	C	0.7513	1533.458	78.23022	C
2028	1432.0	–	D	65.4007	C	0.2551	1468.530	67.06907	C
2029	1437.8	–	D	52.1992	C	0.5060	1510.553	54.84048	C
2030	1443.5	–	D	50.1445	C	0.6991	1544.415	53.65010	C

* C – converged; ** D – diverged.

6. CONCLUSION

The load modelling was evaluated based on real evidence from resident power distribution networks and the load was built using the suggested technique, which successfully depicted realistic loads and produced distribution system's operating features. In this study, we compared newly constructed variations of the NR technique to the existing variants. The convergence behaviour of all techniques was studied using numerical distribution network analyses. The measurements were obtained for STLF and LTLF using a variety of actual loads, including base load and composite loads. In this work, creative techniques were used to handle the OPF problem, such as loadability maximisation for real-time prediction systems employing the CSA. LTLF, STLF and their losses were also presented.

REFERENCES

1. E.O. Kontis, T.A. Papadopoulos, A.I. Chrysochos, G.K. Papagiannis, Measurement-based dynamic load modeling using the vector fitting technique, *IEEE Transactions on Power Systems*, **33**(1): 338–351, 2017, doi: 10.1109/TPWRS.2017.2697004.

2. Y. Adianto, C. Baguley, U. Madawala, N. Hariyanto, S. Suwarno, T. Kurniawan, The coordinated operation of vertically structured power systems for electric vehicle charge scheduling, *Energies*, **15**(1): 27, 2021, doi: 10.3390/en15010027.

3. L. Chávarro-Barrera, S. Pérez-Londoño, J. Mora-Flórez, An adaptive approach for dynamic load modeling in microgrids, *IEEE Transactions on Smart Grid*, **12**(4): 2834–2843, 2021, doi: 10.1109/TSG.2021.3064046.

4. X.-S. Yang, Suash Deb, Cuckoo search via Lévy flights, [in:] *2009 World Congress on Nature & Biologically Inspired Computing (NaBIC)*, pp. 210–214, 2009, doi: 10.1109/NABIC.2009.5393690.

5. Y. Wang *et al.*, Online realization of an ambient signal based load modeling algorithm and its application in field measurement data, *IEEE Transactions on Industrial Electronics*, **69**(7): 7451–7460, 2021, doi: 10.1109/TIE.2021.3102428.

6. H. Gao, C. Koch, Y. Wu, Building information modelling based building energy modelling: A review, *Applied Energy*, **238**: 320–343, 2019, doi: 10.1016/j.apenergy.2019.01.032.

7. P. Regulski, D.S. Vilchis-Rodriguez, S. Djurović, V. Terzija, Estimation of composite load model parameters using an improved particle swarm optimization method, *IEEE Transactions on Power Delivery*, **30**(2): 553–560, 2014, doi: 10.1109/TPWRD.2014.2301219.

8. P. Aree, Aggregating method of induction motor group using energy conservation law, [in:] *10th International Conference on Electrical Engineering/Electronics, Computer, Telecommunications and Information Technology*, pp. 1–5, Krabi, Thailand, May 15–17, 2013, doi: 10.1109/ECTICon.2013.6559506.

9. J.K. Muriuki, C.M. Muriithi, Comparison of aggregation of small and large induction motors for power system stability study, *Global Engineers and Technologists Review*, **3**(2): 9–13, 2013.

10. D. Lew *et al.*, The power of small: the effects of distributed energy resources on system reliability, *IEEE Power and Energy Magazine*, **15**(6): 50–60, 2017, doi: 10.1109/MPE.2017.2729104.

11. S. Eftekharnejad, V. Vittal, G.T. Heydt, B. Keel, J. Loehr, Impact of increased penetration of photovoltaic generation on power systems, *IEEE Transactions on Power Systems*, **28**(2): 893–901, 2012, doi: 10.1109/TPWRS.2012.2216294.

12. D. Krishna, E. Hima Bindu, M. Sasikala, Mathematical modeling and analysis of demand response using distributed algorithm in distribution power system, [in:] *2021 IEEE International Conference on Distributed Computing, VLSI, Electrical Circuits and Robotics (DISCOVER)*, pp. 237–241, 2021, doi: 10.1109/DISCOVER52564.2021.9663598.

13. A. Arif, Z. Wang, J. Wang, B. Mather, H. Bashualdo, D. Zhao, Load modeling – A review, *IEEE Transactions on Smart Grid*, **9**(6): 5986–5999, 2017, doi: 10.1109/TSG.2017.2700436.

14. D. Krishna, M. Sasikala, V. Ganesh, Adaptive FLC-based UPQC in distribution power systems for power quality problems, *International Journal of Ambient Energy*, **43**(1): 1719–1729, 2022, doi: 10.1080/01430750.2020.1722232.

15. S.H. Lee, S.E. Son, S.M. Lee, J.M. Cho, K.B. Song, J.W. Park, Kalman-filter based static load modeling of real power system using K-EMS data, *Journal of Electrical Engineering and Technology*, **7**(3): 304–311, 2012, doi: 10.5370/JEET.2012.7.3.304.

16. F. Aminifar, F. Rahmatian, M. Shahidehpour, State-of-the-art in synchrophasor measurement technology applications in distribution networks and microgrids, *IEEE Access*, **9**: 153875–153892, 2021, doi: 10.1109/ACCESS.2021.3127915.

17. D. Krishna, M. Sasikala, R. Kiranmayi, FOPI and FOFL controller based UPQC for mitigation of power quality problems in distribution power system, *Journal of Electrical Engineering and Technology*, **17**: 1543–1554, 2022, doi: 10.1007/s42835-022-00996-6.

18. B. Singh, R. Mahanty, S.P. Singh, Optimal power flow with benefit maximisation in coordinated bilateral power market, *International Journal of Power and Energy Conversion*, **4**(3): 268–277, 2013, doi: 10.1504/IJPEC.2013.054845.